JOURNAL OF Materials CHEMISTRY

Ionic conductivity, ferroelectricity and chemical bonding in TKWB type ceramics of the $K_6Li_4Ta_{10}O_{30}$–$Pb_5Ta_{10}O_{30}$ system

Virginie Hornebecq,* Jean-Maurice Réau, Antoine Villesuzanne, Catherine Elissalde and Jean Ravez

ICMCB-CNRS-Avenue du Dr. A. Schweitzer-33608 Pessac, France

Received 6th May 1998, Accepted 3rd August 1998

Correlations between Curie temperature and chemical bonding were found in ferroelectric tetragonal potassium tungsten bronze type ceramics [TKWB] using the extended Hückel tight-binding (EHTB) method. The influence of Pb for K,Li substitution is shown. AC complex impedance measurements were performed on ceramics with compositions corresponding to $Pb_{5x}K_{6(1-x)}Li_{4(1-x)}Ta_{10}O_{30}$ (PKLT) in a wide temperature range. The conductivity relaxation parameters of Li^+ conducting PKLT ceramics were determined. Transport properties in these materials appear to be due to a Li^+ ion hopping mechanism. The influence of the substitution $6K^+ + 4Li^+ \rightarrow 5Pb^{2+}$ on the mobility is discussed with the assistance of the results obtained from EHTB calculations.

Introduction

Ferroelectric ceramics are of great interest for applications such as dielectrics for capacitors, infrared detectors, electromechanical converters, electrooptical modulators, *etc.* Dielectric losses often need to be reduced when the sample has to be polarized or for high quality capacitors. In contrast, the conductivity may also be at the origin of other applications such as CTP (coefficient temperature positive), CTN (coefficient temperature negative), microwave absorbants, *etc.* Recent works have therefore been devoted to the study of conductivity in ferroelectrics.[1,2]

The aim of the present work is to prepare and to characterize new ferroelectric ceramics with ionic conductivity only. The cation Ta^{5+}, whose oxidation state is very stable, was chosen to prevent electronic conductivity.

The compositions PKLT selected here belong to the $K_6Li_4Ta_{10}O_{30}$ ($T_c = 7$ K)–$Pb_5Ta_{10}O_{30}$($T_c = 538$ K) system.[3,4]

Furthermore, the relation between the Curie temperature T_c and chemical bonding has been recently determined in ferroelectric perovskites. The approach in the present paper consists firstly of research into the relation between the transition temperature and chemical bonding in TKWB tantalates. Secondly, EHTB calculations were also helpful in understanding the effect of cationic substitution on the Li^+ ionic conductivity.

Preparation

PKLT samples with composition $Pb_{5x}K_{6(1-x)}Li_{4(1-x)}Ta_{10}O_{30}$ are prepared from K_2CO_3, Li_2CO_3, PbO and Ta_2O_5. The cationic substitution corresponds to $6K^+ + 4Li^+ \rightarrow 5Pb^{2+}$. A special process was used in order to keep the initial stoichiometry, in particular to prevent PbO losses by volatilization. Details of the ceramic densification are given elsewhere.[5] The samples are discs of diameter about 7 mm and thickness about 1 mm. X-Ray diffraction analysis revealed the ceramics to be single phase for $0 \leqslant x \leqslant 0.80$. They crystallise with a tetragonal tungsten bronze structure.[6]

Ferroelectric study of PKLT ceramics

Experiments

The dielectric measurements were performed on ceramic discs. Electrodes were formed by depositing gold on the top and bottom of circular surfaces by sputtering. In the 10^2–2×10^5 Hz frequency range, the permittivities were determined, under vacuum, from capacitance and dielectric losses tan δ (the ratio between the imaginary part ε''_r and the real part ε'_r of the relative permittivity) using a Wayne–Kerr Component Analyser Model 6425. The temperature range was 100 to 300 K. The heating rate was close to 0.2 K min^{-1}.

Results

The temperature dependence of the real permittivity ε'_r shows a maximum corresponding to the ferroelectric–paraelectric transition temperature for the various compositions studied ($x = 0.10$; 0.25; 0.50; 0.65; 0.75; 0.80). Fig. 1 gives as an example the curve (ε'_r *versus* temperature) obtained for the composition corresponding to $x = 0.75$ at 10^3 Hz. The transition temperature increases significantly when K^+ and Li^+ are replaced by Pb^{2+} ($6K^+ + 4Li^+ \rightarrow 5Pb^{2+}$). Furthermore, the maximum of ε'_r is wide and implies a diffuse ferroelectric–paraelectric phase transition which can be explained by a domain of variable composition implying a distribution of transition temperatures. Fig. 2 gives the variation of the ferroelectric–paraelectric transition temperature *versus* composition.

Correlation between the Curie temperature and the chemical bonding

Recent works have been devoted to the role of chemical bonding in the Curie temperature and microwave relaxation frequency in tantalates.[7,8] It was shown that, in significantly

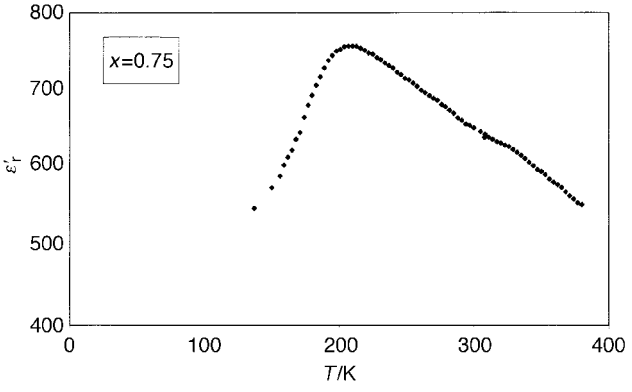

Fig. 1 Temperature dependence of ε'_r ($f = 10^3$ Hz).

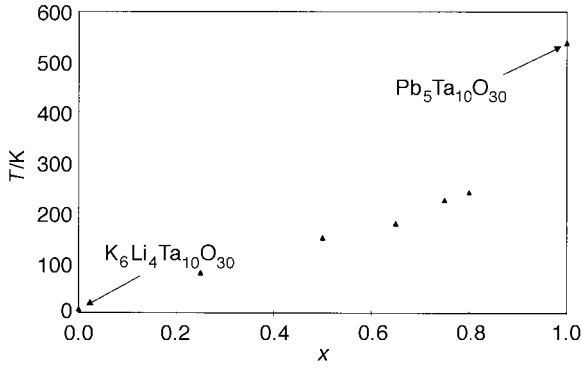

Fig. 2 Composition variation of the ferroelectric–paraelectric transition temperature.

covalent systems such as tantalates and niobates, covalency tends to inhibit the ferroelectric distortion, by strengthening the metal–oxygen bond and stabilizing the paraelectric phase. In tantalates and niobates, this effect appears to dominate the well known softening effect of covalency on short-range interatomic repulsions.[9]

Here, covalency means the amount of mixing of metal d orbitals and oxygen 2p orbitals to form valence bands. This is a more complete view than the one given by electronegativity scales, for which covalency only means the departure from the purely ionic picture. The bond covalencies were evaluated by the computation of crystal orbital overlap populations (COOPs) in the framework of the extended Hückel tight-binding (EHTB) method.[10,11] This quantum chemistry semi-empirical method is particularly well suited for the study of the interplay between chemical bonding and electronic structure of molecules or crystals.[12–17] Valence Slater-type atomic orbitals are attached to each atom; the Fock matrix elements are computed, using the Wolfsberg–Helmholz formula,[18] on the basis of atomic orbital overlaps and tabulated energies. The COOP is the extension to the crystalline solid of the Mulliken overlap population for molecules.[19,20] It is proportional to two quantities closely related to covalency: the overlap of atomic orbitals and the product of the corresponding LCAO coefficients, which is maximal for equal coefficients.

The band structure and the Ta–O and Li–O COOPs were calculated with the EHTB method, for the compositions $K_6Li_4Ta_{10}O_{30}$, $K_4Pb_2Li_2Ta_{10}O_{30}$ and $K_2Pb_4Ta_{10}O_{30}$. The two latter compositions are close to $K_{6(1-x)}Pb_{5x}Li_{4(1-x)}Ta_{10}O_{30}$,

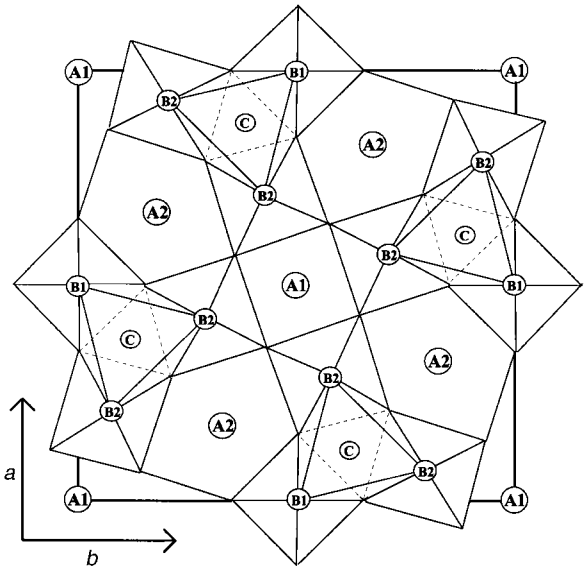

Fig. 3 Structure used to model the TKWB network.

Table 1 Extended Hückel parameters: atomic orbital energies and Slater-type exponents and coefficients. Double-ζ expansions are used for d orbitals

Element	Orbital	H_{ii}/eV	ζ_1	c_1	ζ_2	c_2
Ta	5d	−12.10	4.760	0.6597	1.940	0.5589
	6s	−10.10	2.280	1		
	6p	−6.86	2.241	1		
O	2s	−32.30	2.275	1		
	2p	−14.80	2.275	1		
K	4s	−4.34	1.000	1		
	4p	−2.73	1.000	1		
Pb	6s	−15.70	2.350	1		
	6p	−8.000	2.060	1		
Li	2s	−5.400	0.650	1		
	2p	−3.500	0.650	1		

but correspond to the $K^+ + Li^+ = Pb^{2+}$ substitution mode in $K_6Li_4Ta_{10}O_{30}$. They were chosen in order to define a tractable unit cell for the computation and to allow the study of the Pb for K,Li substitution effects. For ionic radius reasons, Pb atoms were located in the A1 site (C.N. = 12) (Fig. 3) for the second composition and in both A1 and half A2 (C.N. = 15) sites for the third one.

The extended Hückel parameters used in the present work are given in Table 1.

Fig. 4 shows the density of states and COOP curves for $K_4Pb_2Li_2Ta_{10}O_{30}$, calculated with the EHTB method. Li- and K-character bands are located well above the Fermi level E_F and are out of the energy range of this figure. All bonding Pb–O and Ta–O bands lie below E_F; the upper occupied band corresponds to very covalent crystal orbitals with both Pb 6s and O 2p atomic orbital contributions. It is of strong antibonding character against Pb–O bonds. Those very covalent Pb–O interactions are expected to weaken the Ta–O bond covalency.

The COOP values for Ta–O and Li–O bonds, summed up to E_F, are given in Table 2. The COOP, *i.e.* the covalency of Ta–O bonds decreases when the Pb content increases. Moreover, this increase is more significant for those Ta–O bonds close to Pb atoms in the structure (competing bonds effect).[16] This evolution of Ta–O COOPs is due to the decrease of electron density (Fig. 5) along those Ta–O bands affected by the Pb for K substitution. The very low COOP values for

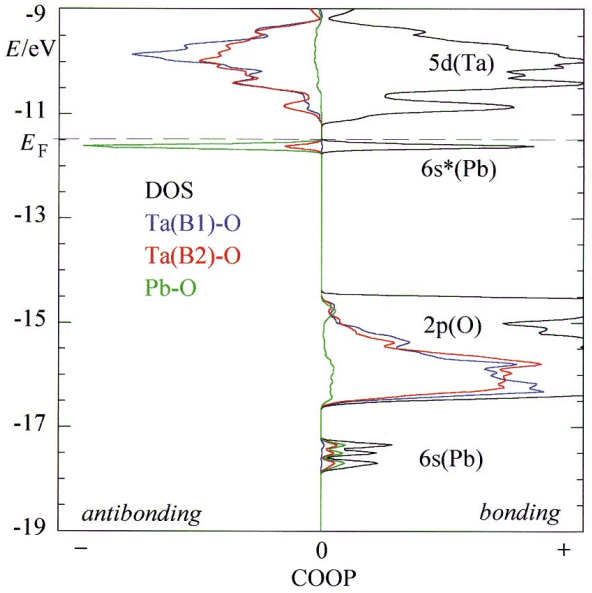

Fig. 4 Density of states and COOP curves for $K_4Pb_2Li_2Ta_{10}O_{30}$. The main atomic orbital contributions to the bands are indicated. 6s and 6s* bands are very covalent with both Pb 6s and O 2p character. B1 and B2 are two crystallographic sites occupied by Ta ions (Fig. 3).

Table 2 COOP values for PKLT ceramics calculated with the EHTB method. B1 and B2 are two crystallographic sites occupied by Ta ions (see Fig. 3)

	COOP (e^-/bond)		
Composition	Ta(B1)–O	Ta(B2)–O	Li–O
$K_6Li_4Ta_{10}O_{30}$	0.6444	0.6299	−0.0111
$K_4Pb_2Li_2Ta_{10}O_{30}$	0.6324	0.5882	−0.0176
$K_2Pb_4Ta_{10}O_{30}$	0.5953	0.5663	

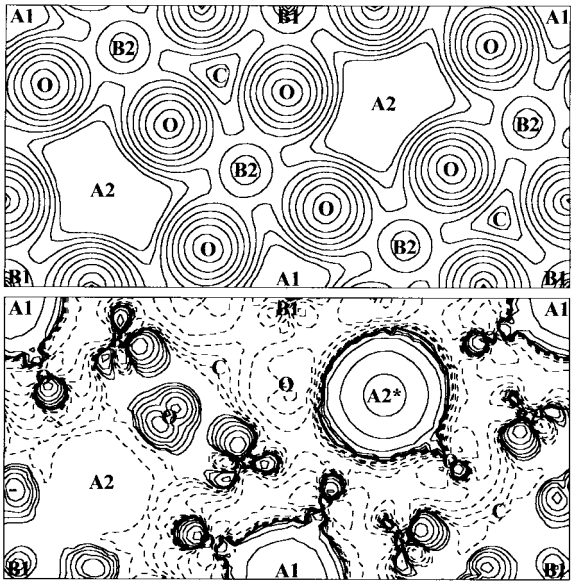

Fig. 5 (Top) Contours (logarithmic scale) of the computed valence electron density for $K_6Ta_{10}O_{30}$. A and B sites are occupied by K and Ta atoms, respectively. The C site is occupied by Li atoms in the PKLT series. K atoms in A1 (A2) sites lie 2.10 Å (2.07 Å) above and 1.83 Å (1.86 Å) below the figure plane. Ta and O atoms lie within 0.16 Å and 0.02 Å from the figure plane, respectively. (Bottom) Contours (logarithmic scale) of the difference in computed valence electron density between $Pb_4K_2Ta_{10}O_{30}$ and $K_6Ta_{10}O_{30}$. Pb atoms are located in A1 and A2* sites. Solid lines: positive values. Dashed lines: negative values.

Li–O bonds confirm their almost purely ionic character; the slight antibonding Li–O interactions (from the covalency point of view) increase with the Pb content.

The COOP evolution with Pb content can be related to the changes of transition temperature. The lowest temperature (7 K) corresponds to the highest Ta–O covalency ($K_6Li_4Ta_{10}O_{30}$); the increase of transition temperature observed upon Pb insertion is correlated to the decrease of Ta–O covalency. This effect was already observed in the $K(Ta_{1-x}Nb_x)O_3$ system and in the comparison of $PbTa_{0.5}Sc_{0.5}O_3$ and $PbNb_{0.5}Sc_{0.5}O_3$; in these significantly covalent systems, the bulk energy stabilisation and the metal–oxygen bond strengthening, due to covalency, tends to inhibit the ferroelectric distortion.[8] The transition temperature can be increased by any chemical means leading to an increase of the metal–oxygen network ionicity.

Impedance study of PKLT ceramics

In the $Pb_{5x}K_{6(1-x)}Li_{4(1-x)}Ta_{10}O_{30}$ solid solution, it is probable that, as in $Ba_5Li_2(Ti_2Nb_8)O_{30}$, Li^+ ions occupy only the triangle sites with 9-fold coordination (sites C).[21] The partial presence of Li^+ ions in those sites is favorable for the occurrence of Li^+ ionic conductivity in the direction parallel to the *c*-axis.

Experiments

AC measurements were performed on the same samples as those used for dielectric measurements; they were carried out under vacuum. Each experimental temperature was maintained by a Eurotherm-902-S Controller for 0.5 hour with an accuracy of ± 0.5 K before collecting data. AC measurements were recorded out using a 1260 Solartron frequency analyser in the frequency range 10^2–10^6 Hz for several temperature cycles between 300 and 700 K.

Results

Complex impedance diagrams of Z''/Ω as a function of Z'/Ω, *i.e.* Cole–Cole plots, are presented in Fig. 6 for the composition corresponding to $x=0.75$ at various temperatures: the bulk ohmic resistance corresponding to each experimental temperature is the intercept on the real axis of the zero phase angle extrapolation of the highest frequency curve.[22,23]

The temperature dependence of conductivity between 300 and 700 K is given in Fig. 7 for some $Pb_{5x}K_{6(1-x)}Li_{4(1-x)}Ta_{10}O_{30}$ compositions as a plot of $\log(\sigma T)$ against inverse temperature: an Arrhenius type behavior is clearly exhibited. A linear fit to $\sigma T=\sigma_0 \exp(-\Delta E_\sigma/kT)$ is shown, with correlation coefficient $R=0.98$. Electrical data relative to the samples are listed in Table 3: a slight increase of activation energy ΔE_σ and a decrease of conductivity can be observed when x increases.

Conductivity relaxation parameters have been calculated from the complex impedance data in the complex modulus formalism $M^*=1/\varepsilon^*=j(\omega C_0)z^*$, where $j^2=-1$, ω ($\omega=2\pi f$) is the angular frequency and C_o is the vacuum capacitance of the cell. This formalism discriminates against electrode polarization and other interfacial effects in solid electrolytes. Plots of normalized modulus (M''/M'_{max}) *versus* $\log(f)$ are given at various temperatures for the composition corresponding to $x=0.75$, for instance, in Fig. 8: the curves are non-symmetric, in agreement with the non-exponential behavior of the conduc-

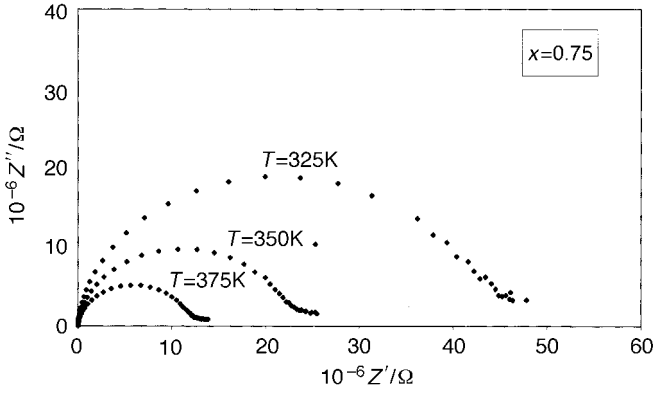

Fig. 6 Complex impedance plots at various temperatures.

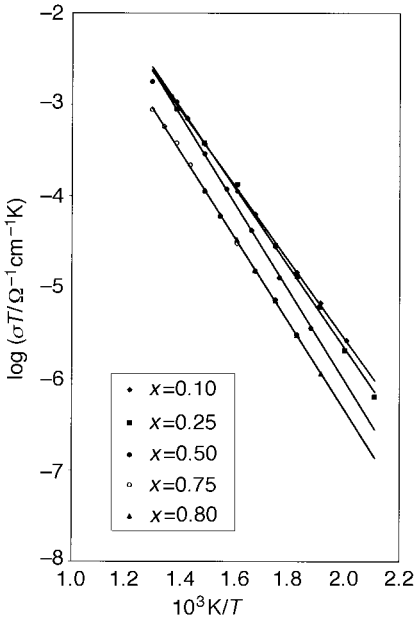

Fig. 7 Inverse temperature dependence of $\log(\sigma T)$ for some $Pb_{5x}K_{6(1-x)}Li_{4(1-x)}Ta_{10}O_{30}$ compositions.

Table 3 Electrical data and conductivity relaxation parameters relative to some various $Pb_{5x}K_{6(1-x)}Li_{4(1-x)}Ta_{10}O_{30}$ compositions studied

	$x=0.10$	$x=0.25$	$x=0.50$	$x=0.75$	$x=0.80$
$\log \sigma_{600K}/\Omega^{-1}$ cm^{-1} (±0.02)	−6.92	−7.05	−7.25	−7.55	−7.58
ΔE_σ/eV (±0.02)	0.84	0.84	0.91	0.92	0.93
$\log \sigma_0/\Omega^{-1}$ cm^{-1} (±0.02)	2.91	2.78	3.17	2.96	3.18
ΔE_f/eV (±0.02)	0.85	0.85	0.93	0.91	0.94
β	0.77	0.76	0.73	0.77	0.74

tivity relaxation, which is well described by the empirical stretched exponential Kohlrausch function $\varphi(t)=\exp[-t/\tau_\sigma]^\beta$ $(0<\beta<1)$.[24–26] In this expression, τ_σ and β are the conductivity relaxation time and the Kohlrausch exponent, respectively. The smaller the value of β, the larger the deviation of the relaxation with respect to a Debye-type relaxation ($\beta=1$). Whatever the temperature, the full width at half-height (FWHH) of the M''/M'_{max} spectrum is wider than the breadth of a Debye peak (1.14 decades) (Fig. 8) and it results in a value of $\beta=1.14/\text{FWHH}$ for the Kohlrausch parameter, which can be considered as independent of temperature in the range studied.

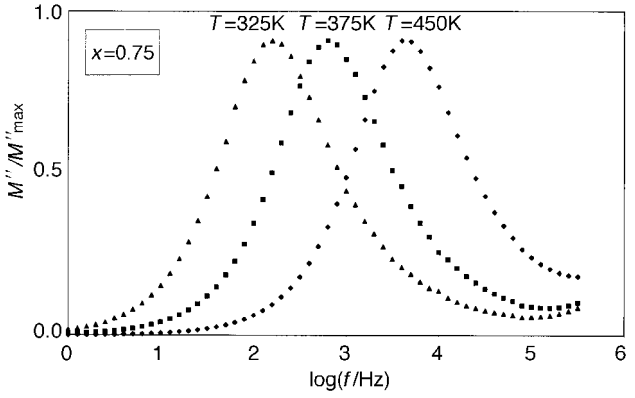

Fig. 8 Plots of normalized modulus (M''/M'_{max}) *versus* $\log f$ at various temperatures.

When the temperature increases, modulus peak maxima shift to higher frequencies (Fig. 8). Fig. 9 gives the temperature dependence of the $f_p=1/2\pi\tau_\sigma$ relaxation frequency relative to M''_{max} for the composition $x=0.75$: Arrhenius-type behavior is shown. The temperature dependence of conductivity is reported in Fig. 9: its behavior is also of Arrhenius-type. Both lines are quasi-parallel, the activation energies issued from the impedance (ΔE_σ) and modulus (ΔE_f) spectra are very similar (Table 3), suggesting that the Li^+ ion transport in the materials studied is probably due to a hopping mechanism.[27] Analogous results were obtained for the other compositions studied (Table 3).

The composition dependence of $\log(\sigma_{600K})$ is given in Fig. 10: $\log(\sigma_{600K})$ slightly decreases, quasi-linearly, when x increases whereas ΔE_σ slightly increases (Table 3). In contrast, the β parameter appears to be independent of x (Table 3). Its value ($\beta\approx0.75$) can be attributed to the existence of a distribution of relaxation times.[28,29] This carrier polarization mechanism appears as weakly dispersive, of the same order of magnitude as the lattice one.[5]

Discussion

Conductivity. For a given ionic conductor, the low frequency limit σ_{dc} of the bulk AC conductivity determined by impedance spectroscopy is governed mainly by the hopping rate of free charge carriers and by the charge carrier concentration $N(T)$:

$$\sigma_{dc}=eN(T)\mu(T)$$

$$\sigma_{dc}=e^2N(T)\gamma a^2_h(v_0/kT)\exp(S_\mu/k)\exp(-E_\mu/kT)$$

where a_h is the hopping distance, γ is a geometrical factor equal to 1/6 for isotropic media, v_0 is an attempt frequency to overcome potential barriers, S_μ is the migration entropy, E_μ is the migration energy, the other parameters having their conventional meaning.[30–32] Equating ΔE_σ to E_μ, the pre-exponential factor σ_0 in the $\sigma T=\sigma_0\exp(-\Delta E_\sigma/kT)$ equation can be given by the following expression:

$$\sigma_0=(e^2a^2_hv_0/6k)N(T)\exp(S_\mu/k)$$

Considering all Li^+ ions as charge carriers in the partial range ($0.10\leqslant x\leqslant0.80$) of the $Pb_{5x}K_{6(1-x)}Li_{4(1-x)}Ta_{10}O_{30}$ solid solution, a maximum of charge carriers could correspond to the composition relative to $x=0.50$ where the C-sites are half-occupied by Li^+ ions. Such a result cannot be deduced from the small composition dependence of $\log(\sigma_0)$ (Table 3), which

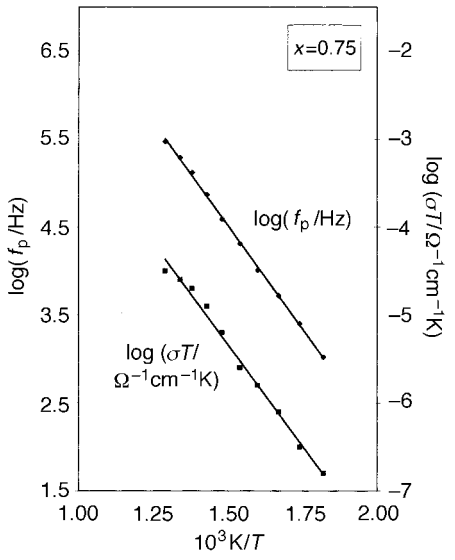

Fig. 9 Temperature dependences of $\log(\sigma T)$ and $\log f_p$, where f_p is the M''_{max} peak frequency.

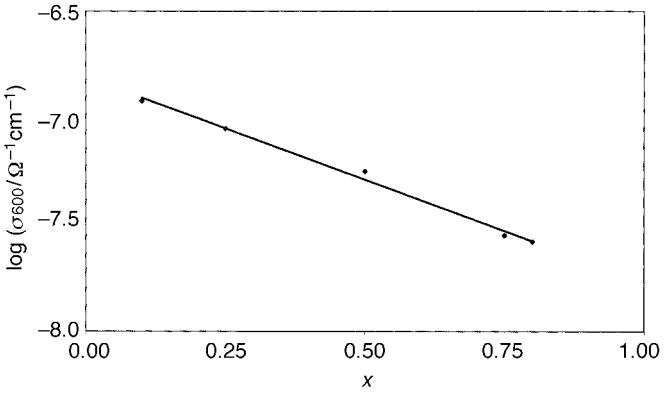

Fig. 10 Variation of log σ_{600K} with x for $Pb_{5x}K_{6(1-x)}Li_{4(1-x)}Ta_{10}O_{30}$.

depends on both charge carrier concentration and migration entropy parameters.

Mobility. Charge density maps were obtained with the EHTB method. Calculations were performed for the $Pb_4K_2Ta_{10}O_{30}$ and $K_6Ta_{10}O_{30}$ compositions, in order to visualise the changes in electron density induced by Pb for K substitution. Li atoms were omitted in these calculations in order to visualise, without the perturbation due to the lithium charge density, the evolution of the electron density in the triangular tunnel section connecting C sites, which will be important in the remainder of this paper. The Fermi level for $K_6Ta_{10}O_{30}$ was located at the top of the 2p oxygen bands in order to reproduce the electron count of $K_6Li_4Ta_{10}O_{30}$.

Fig. 5 shows the calculated valence electron density for $K_6Ta_{10}O_{30}$ in the TaO_2 planes (containing both the equatorial Ta–O bonds and the triangular tunnel sections) and the difference in electron density between $Pb_4K_2Ta_{10}O_{30}$ and $K_6Ta_{10}O_{30}$. No significative valence charge density occurs in A sites for $K_6Ta_{10}O_{30}$ since the 4s and 4p potassium bands are empty. Pb 6s charge density clearly appears in A1 and A2* sites even if Pb atoms are not in the plane of the figure. The decrease of electron density in those Ta–O bonds close to Pb atoms leads to the decrease in the Ta–O COOP calculated above. However, Ta–O bonds close to K atoms appear to be reinforced by the Pb for K substitution. The decrease in electron density in the triangular tunnel section connecting C sites, when the Pb content rises, could play a role in the Li ion mobility.

Several antagonist effects can affect the mobility of Li^+ ions in such a system. Steric effects: (i) a slight decrease of the lattice constants, perpendicular to the tunnel direction, when x increases, leads to a diminution of the tunnel sections containing Li^+ cations.[5] This effect tends to increase the potential barrier and to reduce the mobility of Li^+ cations, but is expected to be weak ($\Delta a/a \approx \Delta b/b < 1\%$); (ii) as Pb is inserted in the network, a transfer of electron density from C-tunnels (around Li atoms) to Pb–O bonds is expected because Pb–O bonds are more covalent than K–O bonds and because Pb^{2+} is more polarizing than K^+ (Fig. 5). Furthermore Pb, K, Li and O atoms are in the same plane (structure). This leads to a higher mobility of Li^+ cations. Electronic effects: (iii) the Li–O COOP has been calculated with the EHTB method (Table 2). It clearly shows that Li–O bond is fully ionic, with a very low antibonding covalent contribution which increases with x, giving a slight increase of Li ion mobility; (iv) from an electrostatic point of view, the replacement of K^+ ions by Pb^{2+} tends to decrease the absolute value of the negative Madelung potential in C-tunnels, because of the difference of charge of the two ions and because the O^{2-} ions net charge is reduced (covalency effect). The electrostatic bonding of Li atoms is then weakened and their mobility increases with x.

The variation of electrical properties inside the $Pb_{5x}K_{6(1-x)}Li_{4(1-x)}Ta_{10}O_{30}$ solid solution is relatively weak. In order to pinpoint precisely the relative importance of various steric and electronic effects, it would be interesting to study the effect of the insertion of lead on compounds containing a same number of Li^+ cations. Work is in progress to correlate insertion of lead, mobility of Li^+ cations and ionic conductivity.

Conclusions

The EHTB method was used to investigate the chemical bonding in TKWB type ceramics. The effect of the Pb for K,Li substitution was studied in PKLT tantalate compounds. Considerations such as covalency allowed us to compare Ta–O bonds in these compounds.

A correlation between chemical bonding and Curie temperature was evidenced: the Curie temperature increases when Pb atoms are inserted in the network. The very covalent lead–oxygen bonds appear to have a significant influence on the metal–oxygen network, decreasing its covalency and favouring the ferroelectric distortion.

Furthermore, the conductivity parameters ΔE_f and β were determined in the complex modulus formalism for various Li^+ containing PKLT ceramics. The activation energies taken from the impedance and modulus spectra are very similar, suggesting that Li^+ ion transport is probably due to a hopping mechanism. The conductivity relaxation is well described by a Kohlrausch function $\varphi(t) = \exp[-t/\tau_\sigma]^\beta$. The value of β ($\beta = 0.75$) can be attributed to the existence of a distribution of relaxation times; it shows that the charge carrier polarization mechanism is weakly dispersive. The effects of the substitution $6K^+ + 4Li^+ \rightarrow 5Pb^{2+}$ on the Li^+ ion mobility were also discussed.

References

1 M. Dong, J. M. Réau, J. Ravez and P. Hagenmuller, *J. Solid State Chem.*, 1995, **116**, 185.
2 M. Dong, J. M. Réau and J. Ravez, *Solid State Ionics*, 1996, **91**, 183.
3 T. Fukuda, *Jpn. J. Appl. Phys.*, 1970, **9**, 599.
4 E. C. Subarrao and G. Shirane, *Acta. Crystallogr.*, 1960, **13**, 226.
5 V. Hornebecq, C. Elissalde, J. M. Réau and J. Ravez, *Phys. Status Solidi*, submitted.
6 A. Magnéli, *Arkiv Kemi*, 1949, **1**, 213.
7 C. Elissalde, A. Villesuzanne, J. Ravez and M. Pouchard, *Ferroelectrics*, 1997, **99**, 131.
8 A. Villesuzanne, C. Elissalde, M. Pouchard and J. Ravez, *Eur. Phys. J. (B)*, in press.
9 R. E. Cohen, *Nature*, 1992, **358**, 136.

10 R. Hoffmann, *J. Chem. Phys.*, 1963, **39**, 1397.
11 M.-H. Whangbo and R. Hoffmann, *J. Am. Chem. Soc.*, 1978, **100**, 6093.
12 R. Hoffmann, *Solids and Surfaces: A Chemist's View of Bonding in Extended Structures*, VCH, New York, 1988.
13 J. K. Burdett and S. A. Gramsh, *Inorg. Chem.*, 1978, **33**, 4309.
14 E. Canadell and M.-H. Whangbo, *Chem. Rev.*, 1991, **91**, 965.
15 J. K. Burdett, *Chemical Bonding in Solids*, Oxford University Press, New York, 1995.
16 A. Villesuzanne and M. Pouchard, *C. R. Acad. Sci. Paris*, 1996, **310**, Série II, 155.
17 A. Simon, *Angew. Chem., Int. Ed. Engl.*, 1997, **36**, 1788.
18 J. H. Ammeter, H.-B. Bürgi, J. C. Thibeault and R. Hoffmann, *J. Am. Chem. Soc.*, 1978, **100**, 3686.
19 T. Hughbanks and R. Hoffmann, *J. Am. Chem. Soc.*, 1983, **105**, 3528.
20 R. S. Mulliken, *J. Chem. Phys.*, 1955, **23**, 1833.
21 M. Dong, Thesis, 1997, Université Bordeaux I, France.
22 K. S. Cole and R. H. Cole, *J. Chem. Phys.*, 1941, **9**, 341.
23 J. E. Bauerle, *J. Phys. Chem. Solids*, 1969, **30**, 2657.
24 G. Williams and D. C. Watts, *Trans. Faraday Soc.*, 1970, **23**, 625.
25 K. L. Ngai and S. W. Martin, *Phys. Rev. B*, 1989, **40**, 10550.
26 F. S. Howell, R. A. Bose, P. B. Macedo and C. T. Moynihan, *J. Phys. Chem.*, 1974, **78**, 639.
27 B. V. R. Chowdari and R. Gopalakrishnan, *Solid State Ionics*, 1987, **23**, 225.
28 B. V. R. Chowdari and K. Radhakrishnan, *J. Non. Cryst. Solids*, 1989, **108**, 323.
29 J. Kawamura and M. Shimoji, *Mater. Chem. Phys.*, 1989, **23**, 72.
30 N. F. Uvarov and E. F. Hairetdinov, *J. Solid State Chem.*, 1986, **62**, 1.
31 D. P. Almond and A. R. West, *Solid State Ionics*, 1987, **23**, 27.
32 N. F. Uvarov, E. F. Hairetdinov, J. M. Réau, J. M. Bobe, J. Sénégas and M. Poulain, *Solid State Ionics*, 1994, **74**, 195.

Paper 8/03412E